

Chapter 2

Simulation and Analysis Methods

The work presented in this thesis focuses on applying the nonadiabatic molecular dynamics simulation methods developed in our group to the photodissociation of solvated I_2^- and on interpreting the results of these simulations. The model itself is the product of many years of toil by Jim Faeder, and his thesis and the publications borne of it are the best references for complete details [1–4]. In this chapter I summarize key features of the method and familiarize the reader with the tools we have developed to understand the dynamics.

In the dynamics of solvated I_2^- , the excess charge on the ion plays a critical role by providing strong coupling between the solute and solvent motion. As the iodine atoms move, the solvent reorganizes so as to solvate the charge. This solvent reorganization in turn polarizes the solute charge distribution. In the representation defined by the electronic states of the isolated solute, this polarization is associated with a strong mixing of the basis states. As we will see, the charge localizes either towards or away from the solvent, depending on the bonding character of the solute electronic state. When the solvent and charge are well separated, the electrostatic attraction produces a strong restoring force which can retard dissociation.

Another interesting aspect of the systems considered here is the similar size of the solute bond strength in the ground electronic state ($D_e = 1.01$ eV), the spin-orbit splitting energy ($\Delta_{so} = 0.94$ eV) and the potential created by the first solvation shell.

This last quantity depends on the solvent and the cluster configuration and in a solvent such as CO₂, roughly half of one solvation shell can generate a potential difference of 0.75–1.0 eV between the two iodine atoms.

These factors produce intriguing dynamics, but also pose a considerable challenge for simulations. We require both detailed information about the solute electronic structure and an interaction potential that depends on all of the nuclear degrees of freedom of the solute–solvent system. We achieve this goal using mixed quantum–classical methods. Throughout the course of a molecular dynamics simulation, the solute electronic structure is determined from an **ab initio** calculation, the nuclear degrees of freedom are treated classically and the interplay between the solute and solvent charge distributions enters through the interaction terms of the effective Hamiltonian described below. The Hamiltonian and its derivatives provide the energies, forces and non-adiabatic transition probabilities necessary to calculate cluster structures and perform molecular dynamics simulations of the complete photodissociation and recombination process.

2.1 Effective Hamiltonian for Solvated I₂[−]

We assume at the outset that there is no charge transfer to the solvent, and electronic structure calculations indicate this is a valid approximation [5, 6]. In our model, the solvent is treated as a perturbation on the solute electronic states. The effects of this perturbation can be strong since the solute states become nearly degenerate. In its simplest form, the effective Hamiltonian is written as a sum of the Hamiltonians of the isolated molecules plus an interaction term:

$$\hat{H}_{eff} = \hat{h}_{solute} + \hat{H}_{solvent} + \hat{H}_{interaction}. \quad (2.1)$$

We assume the excited electronic states of the solvent are not energetically accessible, thus $\hat{H}_{solvent}$ is a constant and may be omitted. The six low-lying electronic states of

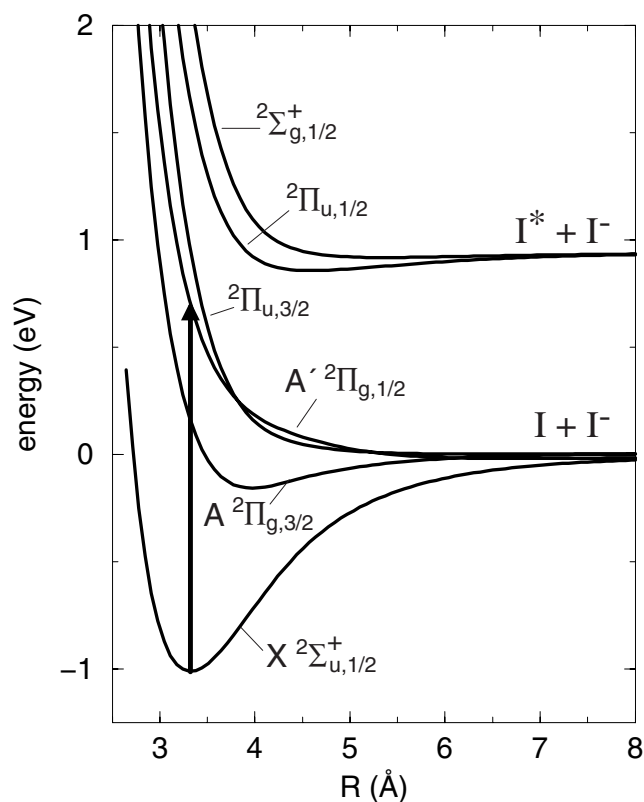


Figure 2.1: Scaled **ab initio** gas phase potential curves for I_2^- . The arrow shows the 790 nm photoexcitation to the $A' \ ^2\Pi_{g,1/2}$ state.

I_2^- , obtained from an **ab initio** calculation of the isolated solute, are the eigenstates of \hat{h}_{solute} and form the basis set in which the total Hamiltonian is evaluated. These states are illustrated in Fig. 2.1. The interaction Hamiltonian includes electrostatic, induction and short range interactions of the solute–solvent system which couple the electronic states of the solute.

Our treatment of the interaction between the solute and solvent charge distributions is based on the distributed multipole (DM) analysis method formulated by Stone [7, 8]. In this representation, a charge distribution is expanded as a sum of charge, dipole and quadrupole moments at multiple sites along the internuclear axis, and the electrostatic interaction between two molecular charge distributions (Q) takes

the form:

$$\hat{E}_{electrostatic} = \frac{1}{2} \sum_{t,u} Q_t^a T_{tu}^{ab} Q_u^b. \quad (2.2)$$

The indices a and b run over all the expansion sites and t and u are the components of the multipole moments (charge, x-dipole, y-dipole, z-dipole,...). All of the dependences on intermolecular distances and orientations are hidden in T_{tu}^{ab} , the interaction tensors, for which explicit formulae have been tabulated [9].

In an adaptation of the DM formalism, we treat the solute charge distribution quantum mechanically while the solvent charges are treated classically. The quantum mechanical analog of the charge density expansion is the distributed multipole **operator**, \hat{q} . The diagonal elements of this operator represent the charge distribution of each electronic state of the solute. A central feature of our treatment is the incorporation of the off-diagonal elements, which represent transition charge densities; in the presence of the solvent they couple the different electronic states giving rise to polarization of the solute [8]. We end up with two types of terms:

$$\hat{H}_{electrostatic} = \frac{1}{2} \mathbf{Q} \cdot \mathbf{T} \cdot \mathbf{Q} + \hat{q} \cdot \mathbf{T} \cdot \mathbf{Q}. \quad (2.3)$$

The first term is the interaction of the permanent moments of the solvent with other solvent molecules. In the second term, \hat{q} is the charge density operator of the solute, and this term represents the full interaction of the solute with the permanent moments of the solvent, including polarizability of the solute.

The solute charge polarizes the charge clouds on the solvent; those induced multipoles interact both with the solute and each other. These effects are described by $\hat{H}_{induction}$. As shown in Ref. [2], the terms of this operator are similar to $\hat{H}_{electrostatic}$,

with the addition of α , the polarizability tensor of the solvent,

$$\begin{aligned}\hat{H}_{induction} = & -\frac{1}{2}\mathbf{Q} \cdot \mathbf{T} \cdot (\mathbf{T} + \alpha^{-1})^{-1} \cdot \mathbf{T} \cdot \mathbf{Q} \\ & -\frac{1}{2}\hat{\mathbf{q}} \cdot \mathbf{T} \cdot (\mathbf{T} + \alpha^{-1})^{-1} \cdot \mathbf{T} \cdot \hat{\mathbf{q}} \\ & -\hat{\mathbf{q}} \cdot \mathbf{T} \cdot (\mathbf{T} + \alpha^{-1})^{-1} \cdot \mathbf{T} \cdot \mathbf{Q}.\end{aligned}\tag{2.4}$$

The first term describes the polarization of the solvent by the permanent moments of other solvent molecules. The second term describes the changes in the solvent charge distribution which are induced by the solute. The third term is a cross term describing polarization by both the solvent moments and the solute charge distribution.

The remaining short range interactions, repulsion and dispersion, are described by pairwise atom–atom potentials fit to reproduce empirical data. Since little is known about the interactions of I_2^- with the solvent molecules, the potentials are fit to the interactions of the solute fragments (I^- and I) and the solvent molecules. These potentials have been characterized by a combination of scattering data and photoelectron spectroscopy [10, 11]. Chapter 7 describes attempts at fitting model parameters for the I_2^- —OCS interaction, for which very little data is available.

2.2 Molecular Dynamics

Our nonadiabatic dynamics simulations are based on the classical path method [12, 13]. We assume the Born-Oppenheimer approximation of separability of nuclear and electronic degrees of freedom holds true, except in regions of strong coupling. The nuclear coordinates evolve classically under the influence of a single potential surface through a short timestep, δt , while the electronic coordinates are integrated quantum mechanically along this path. The timestep for the quantum integration is much smaller than the classical timestep and at each step an assessment is made as to whether the quantum degrees of freedom are in fact separable from the nuclear motion. If necessary,

the classical timestep is reduced, this occurs in regions where transitions are likely. A stochastic algorithm determines when nonadiabatic transitions will occur [14].

The effective Hamiltonian is evaluated in the basis set of the isolated solute at the current geometry. The Hamiltonian matrix is not diagonal due to coupling introduced by the solute-solvent interactions. Diagonalizing the Hamiltonian produces the adiabatic states, $\phi_i(r; R(t))$. These states are functions of all of the electronic coordinates, \mathbf{r} , and depend parametrically on the nuclear coordinates, $\mathbf{R}(t)$. The total wavefunction of the system is a linear combination of these states:

$$\Psi(\mathbf{r}, \mathbf{R}, t) = \sum_i c_i(t) \phi_i(\mathbf{r}; \mathbf{R}(t)). \quad (2.5)$$

Plugging this into the time-dependent Schroedinger equations yields the following equation for the quantum amplitudes, $c_i(t)$,

$$\dot{c}_i(t) = -i c_i H_{ii} + c_i \dot{\mathbf{R}} \cdot \mathbf{d}_{ij}. \quad (2.6)$$

The change in amplitudes depends on the classical velocity and on the nonadiabatic coupling vector, \mathbf{d}_{ij} , the off-diagonal elements of the force matrix. The classical forces and the nonadiabatic couplings can be expressed in terms of derivatives of the Hamiltonian matrix elements, which in turn can be calculated analytically [3].

From the quantum amplitudes, we also compute the probability of making a nonadiabatic transition. This probability is compared to a random number using Tully's method of least switches to determine whether a hop is to be attempted. Each trajectory is in a single quantum state at any given time, and the distribution of states over an ensemble of many trajectories approximates the quantum probabilities given by $|c_i(t)|^2$.

To generate an ensemble of initial conditions, a cluster is first equilibrated using adiabatic dynamics on the ground state with an arbitrary initial structure and fixed total energy. A single long-time trajectory is then sampled to give the initial conditions. The solute is then promoted to an excited electronic state and the trajectories are launched

on the new potential surface. As the dynamics proceeds, the states become coupled and nonadiabatic transitions occur. Trajectories continue until some criterion, for example, a maximum bondlength, is met. The remainder of this chapter deals with interpreting the dynamics.

2.3 Analysis Tools

The benefit of running simulations is the ability to learn, directly, detailed microscopic information about the system. The challenge is to figure out what information is most useful for understanding the dynamics. The photodissociation process takes place on multiple, multidimensional potential energy surfaces. Even with only a few solvent molecules, we cannot possibly visualize all of the degrees of freedom, and even if we could, it's not clear that this picture would provide much enlightenment. Since we expect the most important features of these systems to depend on the overall solvent environment rather than the detailed molecular motions, we define a collective solvent coordinate that depends on the nuclear coordinates of all solvent molecules but condenses that information into a single quantity describing the relative solvation of the two iodine atoms. To understand the forces driving the dynamics requires knowledge of this solvent coordinate, the electronic state and the bondlength of the solute, and the distribution of the excess charge.

A quick way to get acquainted with the dynamics is to watch animations of individual trajectories. It's hard to find a substitute for the intuition that is gained from directly viewing the simulations this way. In addition to watching the nuclear configurations change, it is straightforward to monitor properties such as the electronic state populations and the solute charge distribution. Unfortunately, this process is extremely time-consuming for a large number of trajectories and does not transfer well to print media. More importantly, it is not an effective means for studying the behavior of an entire ensemble because it is too easy to be distracted by the frequently irrelevant partic-

ulars of individual trajectories. Nevertheless, when unanticipated results are observed it is often necessary to resort to this tool and some of our most significant results were initially discovered in this way. (In the long run, it would be worthwhile to create a user interface to display multiple aspects of a trajectory onscreen simultaneously, now that we know what data to look at.)

When the results of a new calculation are in, the first step is to analyze the ensemble as a whole with methods that have proven useful in previous studies. At the early stages of this project, that essentially meant comparing final product distributions to experimental values and watching individual trajectories. Since any system of interest differs from what's been done before, the next task is to identify aspects of the dynamics which are surprising or unusual and then to design new tools that characterize them well enough to allow one to quickly identify additional instances in the entire ensemble.

2.3.1 Potential Energy versus Time

The eigenvalues of the Hamiltonian matrix, which are automatically generated during the course of the simulations, are the instantaneous energies of the electronic states. A plot of the energies of all of these states (not just the one that is occupied) along a simulation trajectory can be used to reveal several aspects of the dynamics. Figure 2.2 shows such a plot for I_2^- embedded in a CO_2 cluster. For simplicity, we will not worry about which electronic state is occupied. Initially, the energetic ordering of the states is the same as in isolated I_2^- , namely, X , A , A' , a , a' and B , from the lowest to the highest energy. The first few hundred femtoseconds of a trajectory are dominated by the impulsive dissociation of I_2^- as it races down a repulsive electronic state and the potential energy traces resemble a compressed version of the solute potential curves shown in Fig. 2.1. Commonly, we see evidence of kinematic caging as I_2^- recoils from the solvent cluster. In the trajectory shown, the sharp spike occurring simultaneously in

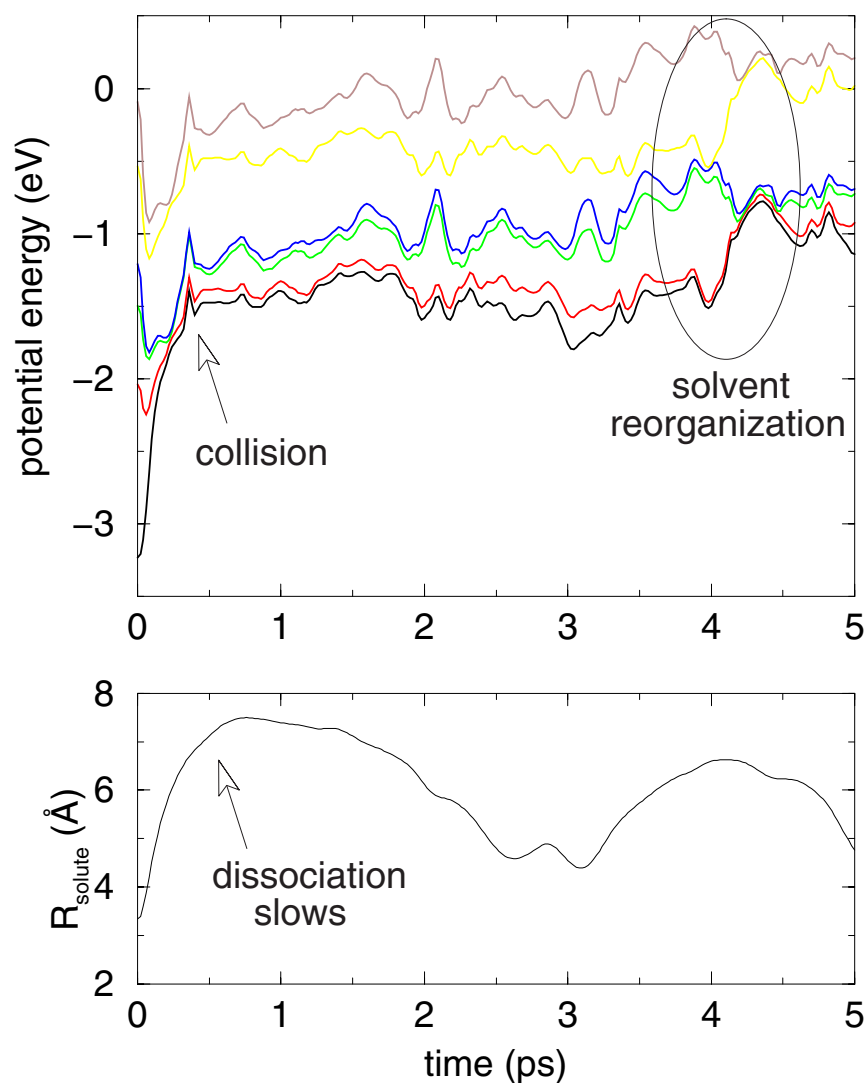


Figure 2.2: The top panel shows the potential energy versus time for the 6 electronic states of I_2^- included in our simulations. The bottom panel shows the solute bondlength versus time for the same trajectory.

all of the electronic states, just before 0.5 ps, is due to a strong collision with the solvent cage. The solute bondlength for this trajectory, plotted in the lower panel of Figure 2.2, corroborates this interpretation, as does an animation of the dynamics (not shown).

For the next several picoseconds of this trajectory, the solute bondlength varies, but generally remains large enough that the contributions to the energy from the solute potential are roughly constant. The small-scale fluctuations of the energy depend on

microscopic details of the positions of each atom in the cluster, and are not of much interest. The intriguing behavior is the changing pattern of nearly degenerate states [15]. Between 0.5 and 1.5 ps, there are essentially four energy levels, the lower two being doubly degenerate. Note that the spacing between the two upper states mimics the spacing between the two lower states, while a larger gap tends to separate the second and third levels. This classification is approximate and subjective, but is substantiated by considering the behavior of a large number of trajectories. From 1.5 to 3.5 ps the potential energy details are complicated by changes in the solute bondlength, but the underlying pattern is maintained. At about 4 ps something very interesting happens. A pattern of 3 distinct levels forms, but quickly gives way to a new pattern with two levels. This latter combination of states corresponds to the two lowest dissociative limits of I_2^- , separated by the spin-orbit splitting of iodine (0.94 eV). These dramatic changes in the spacings between electronic states are accompanied by significant changes in the solvent environment. In time, we will come to see how the optimal solvent configuration depends on the occupied electronic state and thus understand the driving forces behind these large scale reorganization events. While these plots provide initial insights into the dynamics, they are limited in their usefulness because the potential energy of the system depends on so many variables, and we need to develop another method for analyzing the dynamics.

2.3.2 The Solvent Coordinate

To visualize how the cluster configuration is changing in time, without getting bogged down in the details of each molecular motion, we introduce a collective solvent coordinate inspired by the theory of electron transfer in liquids [16–18]. The solvent coordinate, $\Delta\Phi$, is defined as the change in energy when a charge of $-e$ is moved from one iodine atom to the other, holding all nuclear coordinates fixed. When the magnitude of $\Delta\Phi$ is small, as in Fig. 2.3(a), the two iodine atoms are exposed to similar solvent

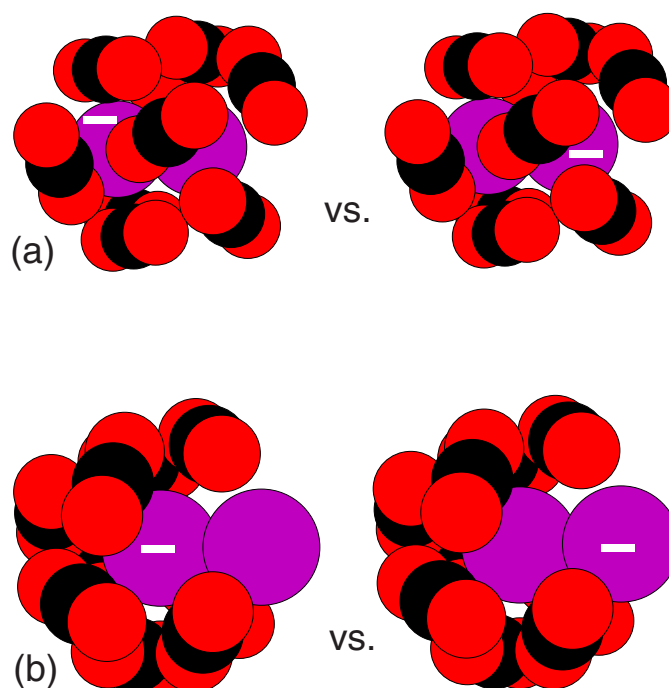


Figure 2.3: The solvent coordinate. (a) Solvent evenly distributed between iodine atoms, small $\Delta\Phi$. (b) Anisotropic solvent distribution, large $\Delta\Phi$.

environments, and when the magnitude of $\Delta\Phi$ is large, as in Fig. 2.3(b), the two iodine atoms are exposed to very different solvent environments. We refer to these two cases as symmetric and asymmetric solvation, respectively.

While $\Delta\Phi$ depends on the cluster geometry, it is a measure of the energy of that configuration, not a direct specification of the nuclear coordinates. Many different cluster configurations can have the same solvent coordinate. Also, in strongly interacting solvent clusters, such as CO_2 , very small changes in the nuclear configuration can lead to large changes in the solvent coordinate, as we will see in Chapters 3 and 4.

The asymmetry of the solvent cluster, as measured by this coordinate, is a principal factor in determining the relative energy spacings between the solute electronic states and the location of strong nonadiabatic coupling regions. This is implicit in the plot of the potential energy shown above, but we will develop better tools for examining the role of the solvent coordinate below.

2.3.3 Solute Charge Flow

To study the flow of the excess solute charge, in relation to the overall solvent environment, we compare the solvent asymmetry coordinate, $\Delta\Phi$, defined above, with an analogous coordinate that specifies the location of the charge. The quantity Δq is the charge differential between the two iodine atoms,

$$\Delta q = |q_1| - |q_2|. \quad (2.7)$$

When Δq is positive, atom 1 has the bulk of the charge; when Δq is negative, atom 2 has the bulk of the charge and when Δq is zero the charge is completely delocalized. Likewise, the quantity, $\Delta\Phi$ is the difference in the solvent potential at the two iodine atoms. When $\Delta\Phi$ is positive, atom 1 is more heavily solvated, and so forth. We then consider the product, $\Delta q\Delta\Phi$, which is positive when the charge and solvent cluster are localized on the same iodine nucleus. This situation, which we are accustomed to assuming, is referred to as normal charge localization (or flow). If the product of Δq and $\Delta\Phi$ is negative, the charge has localized on the **less**-solvated iodine nucleus. In this case, which we call anomalous charge flow, it is important to note that the solvent continues to seek out the charge; it is the motion of the quantum mechanical electron which seems counterintuitive. As discussed in the next chapter, anomalous charge flow is a general characteristic of antibonding electronic states.

The fact that these two kinds of charge localization can occur is an important clue for unraveling the relationship between the solvent coordinate and the potential energy of the system, as depicted in Fig. 2.2. By constructing this measure of the charge flow, we have encapsulated an enormous amount of information about the kinds of dynamics we can expect on a particular electronic state. In the final section of this chapter, we describe a way to visualize the dynamics of many trajectories at once. Then we will be prepared to examine the actual simulations.

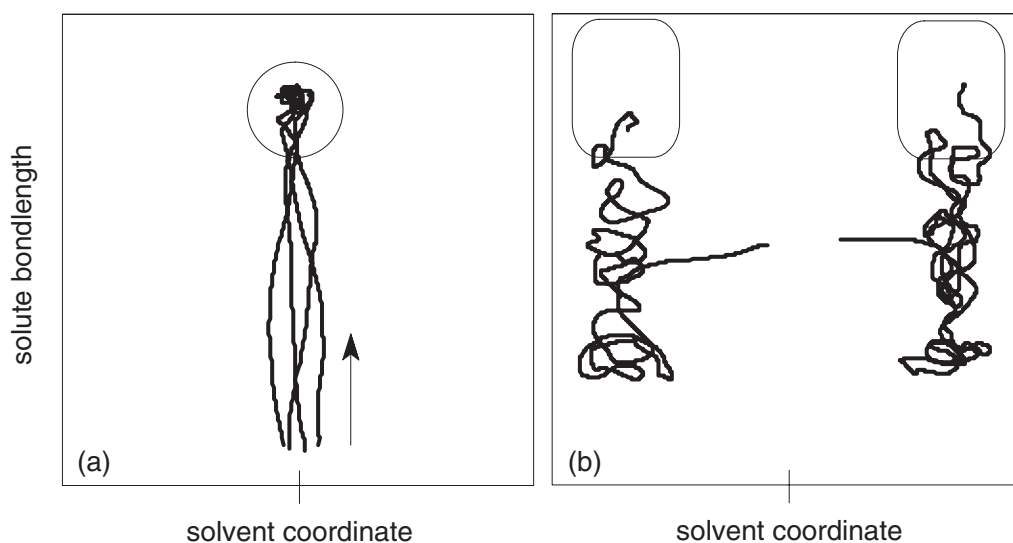


Figure 2.4: Two-dimensional map of trajectories on two different types of electronic states. (a) Initially, trajectories are straight or smooth and move collectively towards large solute bondlengths, reflecting the repulsive nature of this electronic state. (b) Trajectories on a potential surface similar to the one shown in Fig. 2.5(b). The nonadiabatic coupling regions are circled and the motion of trajectories in these regions is discussed in the text.

2.3.4 Two-dimensional Maps

We have found that the primary effect of the solvent is to produce an asymmetric environment around the solute. The Marcus solvent coordinate, $\Delta\Phi$, originally developed for the theory of electron transfer in solution, provides a convenient, overall measure of this asymmetry. One may envision the dynamics as being dominated by a two-dimensional effective Hamiltonian parametrized by the solute bondlength, R , and the solvent coordinate, $\Delta\Phi$ [19–21]. In so far as this is valid, the trajectories move on the two-dimensional potential surface associated with this Hamiltonian. In our analysis, we do not actually construct these surfaces; instead we plot the trajectories using these two coordinates and infer the shapes of the potential surfaces from the patterns that emerge. We emphasize that the dynamics is always computed from simulations that include all of the degrees of freedom present and the two-dimensional representation is used only as an analysis tool.

Plots of this variety proliferate throughout the remaining chapters and the following is a guide for inferring the shape of the potential energy surfaces from the trajectories. To indicate the electronic state of the solute, we typically use multiple linestyles or plot the population of each state on a separate graph. The potential energy curves of isolated I_2^- shown in Fig. 2.1 are a guide to the forces acting along the solute bond. These curves are most useful at short bondlengths (2–4 Å), where the potential energy of the entire system depends more strongly on R than on $\Delta\Phi$. For example, Fig. 2.4(a) shows a number of trajectories starting on a repulsive electronic state at a short bondlength with a distribution of solvent coordinates near zero. Early on, the bondlength increases (repulsive state) with very little influence from the solvent. At some point, dissociation is stopped by the solvent. The trajectories then collect in a basin on the potential surface, taking on a snarled appearance. In the absence of surface hopping they would be trapped here. Introducing nonadiabatic coupling is like perforating the basin; clusters can now drop down to lower electronic states. The key point, however, is that smooth or straight sections in the trajectories reveal regions of the potential surface that are steeply sloped.

Figure 2.5(a) illustrates a case where the forces within the solute are weak, so that the bondlength is largely irrelevant and the solvent coordinate directs the dynamics. Trajectories enter this region at a variety of bondlengths with near-zero solvent coordinates and rapidly move to large solvent coordinates. The ridge in the potential energy surface that would produce this behavior is shown qualitatively. Figure 2.5(b) shows trajectories sliding down from a ridge and then becoming tangled, filling out a U-shaped region. This diffusive motion indicates the trajectories have reached a nearly flat region of the potential energy surface. In regions such as this, the dynamics reflect the competition between solvation forces which act to localize the excess charge and chemical bonding forces which act to delocalize the excess charge. With a map of an ensemble of trajectories, one can assess which force is stronger. If trajectories readily

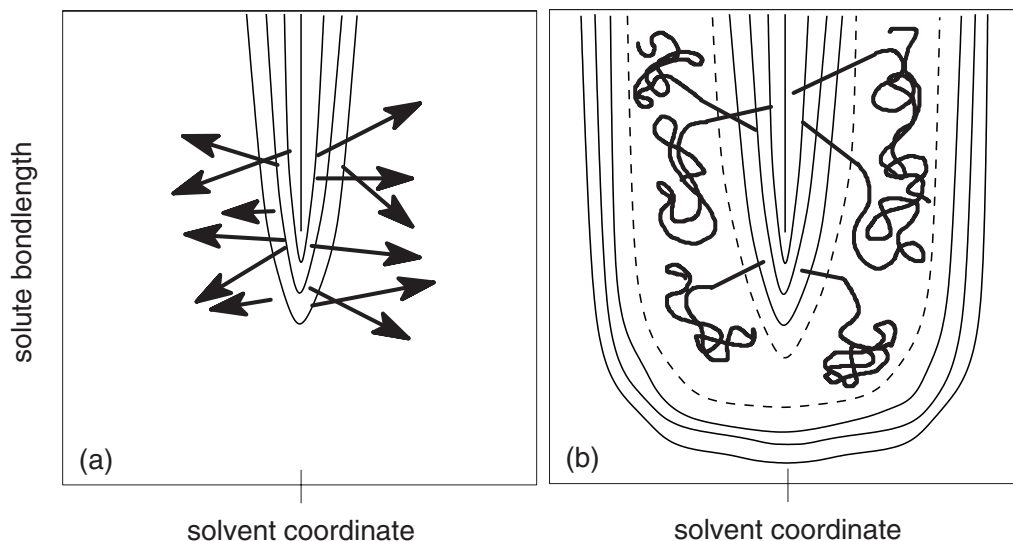


Figure 2.5: Two-dimensional map of trajectories exploring an electronic state. Heavy lines show the course of the dynamics, thin lines are attractive (dashed) and repulsive (solid) contours of the potential surface. (a) Trajectories racing down from the top of a steep ridge. (b) As the trajectories continue, more is revealed about the potential surface. Here the ridge leads to a trough.

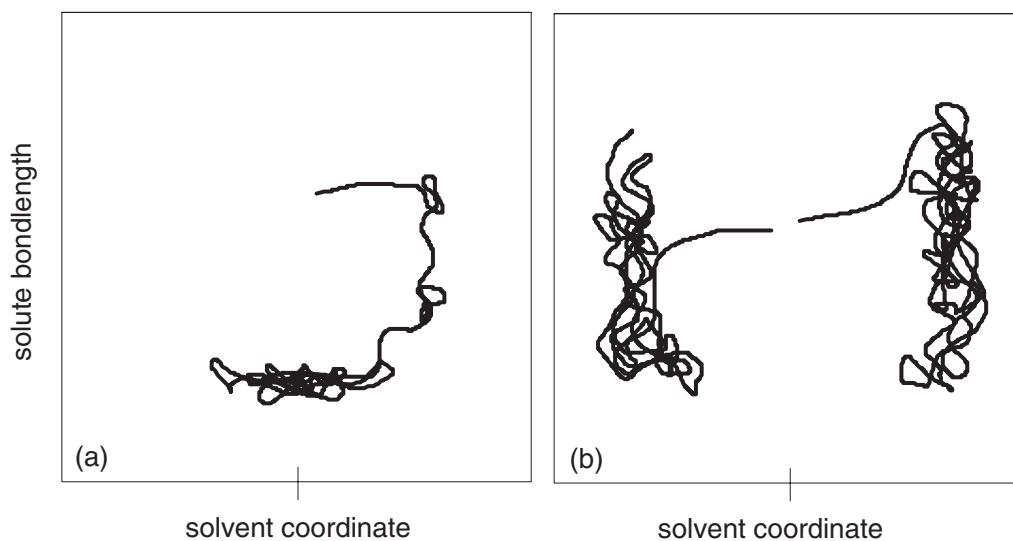


Figure 2.6: Two-dimensional map of trajectories illustrating the competition between the solute bond and solvation forces. The underlying potential surface is similar to the one shown in Fig. 2.5(b). (a) Trajectory fluctuates around zero solvent coordinate at a short bondlength, indicating a stable bond. (b) Trajectories do not cross through zero solvent coordinate, indicating that the solvent forces prevent the solute bond from forming.

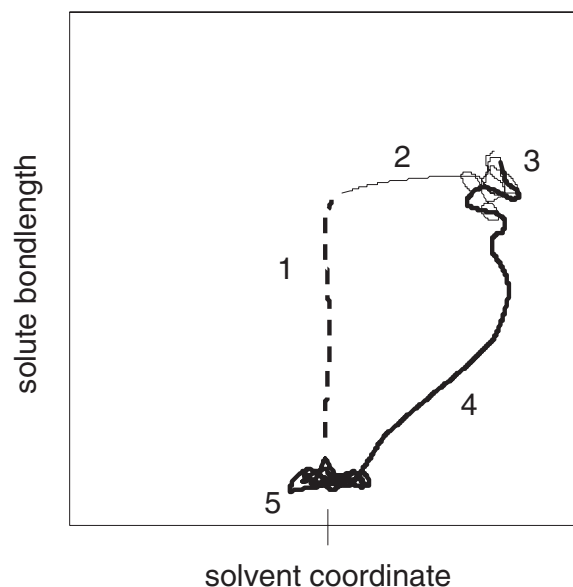


Figure 2.7: Two-dimensional map of a trajectory showing the complete dissociation and recombination process on three different electronic states, indicated by different linestyles. The trajectory proceeds from 1 to 5. The potential surfaces which we infer from these dynamics are described in the text.

cross $\Delta\Phi = 0$, as in Fig. 2.6(a), it indicates that the I_2^- bond has reformed. In contrast, a double wellled map as in Fig. 2.6(b), indicates that strong solvation forces prevent recombination of the solute.

The nature of nonadiabatic coupling regions can also be inferred from these maps. Two distinct types of transition regions are shown in Fig. 2.4. In the first case, Fig. 2.4(a), the potential surface near the coupling region of the initial state is bowl-shaped and trajectories are essentially trapped here until a nonadiabatic transition occurs. In the second case, Fig. 2.4(b), the potential surface of the initial state is nearly flat. Here there are no forces restricting the trajectories to the coupling region. Commonly, repeated attempts are necessary before a hop is successful and so transitions from this second type of coupling region may be much less frequent since trajectories may wander away before a transition occurs.

Figure 2.7 shows a complete trajectory illustrating key points regarding these

plots. Sections of the trajectory are labelled 1–5 and linestyles indicate different electronic states. I. When the potential surface is steep, trajectories are straight or very smooth (1,2,4). II. Tangled trajectories indicate troughs or wells on the surface (3,5). III. Dramatic changes in the solvent coordinate coincide with transitions between states of different charge switching character (2) and when travelling on a single state between regions of strong solvation and strong bonding (4).

Once accustomed to reading data from these plots, it is easy to design a wide variety of diagnostic tools which exploit the dense concentration of information that can be presented this way. In one such application, we plot a point in the $(R, \Delta\Phi)$ plane to represent the nuclear configuration of each cluster in the ensemble and then animate these points to follow the trajectory of each cluster throughout the photodissociation process. This allows us to identify times and places where substantial fractions of the ensemble arrive in unison. Locating these pile-ups in the population distribution is a preliminary step to understanding the spectroscopy of the excited clusters. Another map can be constructed by highlighting regions where the energy gap between a pair of states matches a chosen value. If we overlay the map and the animation, we can see how the population passes through an absorption window. This is just a few short steps away from actually simulating the absorption recovery signal.

Throughout the remaining chapters, additional analysis methods built from the basic elements described here are used to explore the dynamics simulations. Most notably, Chapter 3 introduces a view of the dynamics based on the Marcus theory of electron transfer and this is developed in greater detail in Chapter 4. The methods for simulating the absorption recovery signal are found in Chapter 5.

References for Chapter 2

- [1] J. Faeder, The X₅⁻ Files: Modeling Structure and Dynamics of Solvated Molecular Ions, PhD thesis, University of Colorado, 1998.
- [2] P. E. Maslen, J. Faeder, and R. Parson, *Mol. Phys.* **94**, 693 (1998).
- [3] J. Faeder, N. Delaney, P. Maslen, and R. Parson, *Chem. Phys.* **239**, 525 (1998).
- [4] P. E. Maslen, J. Faeder, and R. Parson, *Chem. Phys. Lett.* **263**, 63 (1996).
- [5] A. Sanov and W. C. Lineberger, private communication.
- [6] A. Sanov, J. Faeder, R. Parson, and W. C. Lineberger, Spin-orbit coupling in ICO₂ and IOCS van der waals complexes: Beyond the pseudo-diatomic approximation, 1999, in press.
- [7] A. J. Stone, *Chem. Phys. Lett.* **83**, 233 (1981).
- [8] A. J. Stone, The Theory of Intermolecular Forces, Oxford, New York, 1996.
- [9] S. L. Price, A. J. Stone, and M. Alderton, *Mol. Phys.* **52**, 987 (1984).
- [10] Y. Zhao, C. C. Arnold, and D. M. Neumark, *J. Chem. Soc. Faraday Trans.* **89**, 1449 (1993).
- [11] Y. Zhao, I. Yourshaw, G. Reiser, C. C. Arnold, and D. M. Neumark, *J. Chem. Phys.* **101**, 6538 (1994).
- [12] J. C. Tully, Nonadiabatic processes in molecular collisions, in Dynamics of Molecular Collisions, edited by W. H. Miller, volume Part B, Plenum, New York, 1976.
- [13] S. Hammes-Schiffer, *J. Phys. Chem. A* **102**, 10444 (1998).
- [14] J. C. Tully, *J. Chem. Phys.* **93**, 1061 (1990).
- [15] C. Margulis and D. F. Coker, *J. Chem. Phys.* **110**, 5677 (1999).
- [16] R. A. Marcus, *Ann. Rev. Phys. Chem.* **15**, 155 (1964).

- [17] M. D. Newton and N. Sutin, *Ann. Rev. Phys. Chem.* **35**, 437 (1984).
- [18] G. C. Schatz and M. A. Ratner, Quantum Mechanics in Chemistry, chapter 10, Prentice Hall, Englewood Cliffs, 1993.
- [19] R. Bianco and J. T. Hynes, *J. Chem. Phys.* **102**, 7885 (1995).
- [20] I. Benjamin, P. F. Barbara, B. J. Gertner, and J. T. Hynes, *J. Phys. Chem.* **99**, 7557 (1995).
- [21] P. K. Walhout, J. C. Alfano, K. A. M. Thakur, and P. F. Barbara, *J. Phys. Chem.* **99**, 7568 (1995).